HHS Public Access

Author manuscript

Nat Chem Biol. Author manuscript; available in PMC 2020 August 01.

Published in final edited form as:

Nat Chem Biol. 2019 August ; 15(8): 786–794. doi:10.1038/s41589-019-0322-6.

Specificity for latent C-termini links the E3 ubiquitin ligase CHIP to caspases

Matthew Ravalin[1], **Panagiotis Theofilas**[3], **Koli Basu**[1], **Kwadwo A. Opoku-Nsiah**[1], **Victoria A. Assimon**[1], **Daniel Medina-Cleghorn**[1], **Yi-Fan Chen**[1,6], **Markus F. Bohn**[1], **Michelle Arkin**[1], **Lea T. Grinberg**[2,3,4,5], **Charles S. Craik**[1,7], **Jason E. Gestwicki**[1,2,7]

[1]Department of Pharmaceutical Chemistry, University of California at San Francisco, San Francisco, CA, USA.

[2]Sandler Neuroscience Center, University of California at San Francisco, San Francisco, CA, USA.

[3]Department of Neurology, Memory and Aging Center, University of California at San Francisco, San Francisco, CA, USA.

[4]Department of Pathology, University of California at San Francisco, San Francisco, CA, USA.

[5]Global Brain Health Institute, University of California at San Francisco, San Francisco, CA, USA.

[6]University of California San Francisco Summer Research Training Program

Abstract

Protein-protein interactions between E3 ubiquitin ligases and protein termini shape the proteome. These interactions are sensitive to proteolysis, which alters the ensemble of cellular N- and C-termini. We have identified a mechanism wherein caspase activity reveals latent C-termini that are recognized by the E3 ubiquitin ligase CHIP. We expanded established CHIP specificity and identified hundreds of putative CHIP interactions arising from caspase activity. Subsequent validation confirmed that CHIP binds the latent C-termini at tau^{D421} and caspase-6^{D179} *in vitro* and in cells. CHIP binding to tau^{D421}, but not tau^{FL}, promotes its ubiquitination, while binding to caspase-6^{D179} mediates ubiquitin-independent inhibition. Given that caspase activity generates tau^{D421} in Alzheimer's Disease (AD), these results suggest a concise model for CHIP regulation of tau homeostasis. Indeed, we find that a loss of CHIP expression in AD coincides with the accumulation of tau^{D421} and caspase-6^{D179}. These results illustrate an unanticipated link between caspases and protein homeostasis.

[7]Correspondence to: Charles.Craik@ucsf.edu or Jason.Gestwicki@ucsf.edu.

Author contributions: M.R., C.S.C. and J.E.G designed the studies and wrote the manuscript. M.R., K.A.O., V.A.A., Y.C. and D.M.C., conducted biochemistry experiments and generated necessary reagents. K.B., M.F.B. and M.R. designed and executed structural and computational studies. M.R. and D.M.C. designed and conducted cell biology experiments. P.T. and L.T.G designed and conducted the immunohistochemistry experiments. J.E.G, C.S.C., M.A. and L.T.G. provided funding.

Data availability: All structural data has been deposited in the PDB (PDB ID 6EFK and 6NSV). All predicted CHIP binders and relevant scores are provided in the Supplementary Information. Additional data supporting the findings of this manuscript are available from the corresponding author upon reasonable request.

Competing interests: None declared

Introduction

An important subset of protein-protein interactions (PPIs) involve the recognition of a free amino (N) or carboxy (C) terminus by a binding partner[1–3]. This type of PPI is sensitive to proteolysis, which irreversibly modifies the chemical composition of a protein's terminus. Indeed, proteolysis can initiate binding events at protein termini and subsequently activate signaling cascades, including protease-activated receptor (PAR) signaling, apoptosis, and the unfolded protein response[4–6]. Similar recognition events are important in maintenance of protein homeostasis (a.k.a. proteostasis). E3 ubiquitin ligases provide specificity to the ubiquitin proteasome system (UPS) by linking substrate-recognition and ubiquitination[7]. A subset of E3 ubiquitin ligase recognition domains are selective for protein termini; for example, the E3 ubiquitin ligases of the N-end rule pathways (*e.g.* the UBR E3 ligases) recognize N-termini bearing specific amino acids (N-degrons), prioritizing them for destruction via the UPS[8,9]. In the N-end rule, proteolysis by methionine aminopeptidases plays a critical gatekeeping role by removing stabilizing N-terminal methionine residues to reveal UBR binding motifs[10,11]. Analogous recognition of C-termini by adaptor proteins to Cullin-RING E3 ubiquitin ligases has recently been shown to couple C-terminal recognition to turnover, perhaps through a protease-dependent pathway[12,13]. Additionally, E3 ubiquitin ligases that recognize protein termini are central to the regulation of cell survival. Specifically, XIAP is a RING E3 ubiquitin ligase that inhibits the cystine proteases, caspase-3, −7 and −9[14]. This inhibition deters the activation of apoptosis in a healthy cell. However, upon activation of apoptotic pathways, second mitochondrial activator of caspases (SMAC) is cleaved by the mitochondrial protease, PARL, allowing the free N-terminus of SMAC to sequester the inhibitory domain in XIAP[15,16]. Through these mechanisms, proteases enable recognition of latent termini to regulate critical cellular processes.

Here, we report a protease-coupled recognition event wherein caspase activity reveals latent C-termini that are bound by carboxy-terminus of Hsp70-interacting protein (CHIP). CHIP is a homodimeric E3 ubiquitin ligase that contains a Ubox domain and a tetratricopeptide repeat (TPR) domain[17,18]. The TPR domain was thought to be selective for the (I/M)EEVD motif present at the C-terminus of cytosolic members of the heat shock protein 70 (Hsp70) and 90 (Hsp90) families. These interactions favor the ubiquitination and turnover of both the chaperones and chaperone-bound substrates[19,20]. Moreover, similar TPR domains are found in other Hsp70/Hsp90 co-chaperones such that competition for chaperone is thought to direct client fate[21,22]. Here, we find that CHIP's TPR domain has a broader specificity than previously appreciated, so that hundreds of latent C-termini may compete with Hsp70/Hsp90 in the context of caspase activation. We show that caspase cleavage of microtubule-associated protein tau (MAPT/tau) generates a high-affinity CHIP ligand. Strikingly, CHIP mediates *in vitro* poly-ubiquitination of cleaved tau (tau^{D421}), but not full-length tau (tau^{FL}), without the need for chaperone. In addition, we find that cleavage of caspase-6 during its maturation generates a strong CHIP recognition motif, which mediates potent ubiquitin-independent inhibition of caspase-6^{D179}. As both tau and caspase-6 cleavage are linked to AD, these findings suggested a possible feedback mechanism that links tau proteostasis and cell survival. In support of this model, we find that CHIP levels are decreased during progression of AD in patients, concomitant with an increase in cleaved tau^{D421} and active

caspase-6^{D179}. These results point to a much broader role for CHIP than its classical collaboration with Hsp70s/Hsp90s.

Results

CHIP TPR domain specificity extends beyond chaperones

Co-crystal structures have shown that Hsp70's IEEVD motif binds to a groove in CHIP's TPR domain, such that the two carboxylates of the C-terminal Asp form a bidentate interaction with CHIP's carboxylate clamp formed by residues Lys30 and Lys95 (Fig 1a)[23]. This interaction is common among TPR co-chaperones (Fig 1b). In addition, previous mutagenesis studies have identified the P5 (Ile in Hsp70s or Met in Hsp90s), P2 (Val), and P1 (Asp) as the critical positions for affinity and specificity[24]. However, the global binding specificity of CHIP's TPR domain has not been explored. To achieve this, we designed a positional scanning synthetic combinatorial library (PSSCL) of acetylated five amino acid peptides[25,26]. In this library, we fixed the C-terminal amino acid as an Asp and synthesized pools of peptides in which a second position was fixed, while each of the others contained a mixture of the twenty proteinogenic amino acids (see Methods). The resulting library consisted of eighty pools of eight thousand peptide sequences, each with two fixed positions (Fig 1c). To measure binding, we used two approaches. In the first, we determined the change in thermal stability (T_m) of CHIP in the presence of peptide pools by differential scanning fluorimetry (DSF) (Supplementary Fig 1). We then confirmed these findings in fluorescence polarization (FP) experiments by measuring the capacity of each peptide pool to displace FP tracers derived from either the Hsc70 (HSPA8) or Hsp90α (HSP90AA) sequences (Supplementary Fig 2). These experiments reproduced the known determinants of chaperone binding to CHIP's TPR domain and the results from the three biochemical platforms correlated well with each other (Fig 1d). In addition to the established specificities mentioned above, we identified unexpected preferences for Leu at P5, aromatic amino acids at P4, bulky residues at P3 and Pro at P2. Interestingly, we found that the best-known CHIP TPR binder (Hsp70's IEEVD) was sub-optimal at all four positions queried. Using this information, we synthesized an optimized FP tracer (CHIPOpt; FITC-Ahx-LWWPD) and found that it bound CHIP with an apparent pKd of 7.8 ± 0.1 (Fig 1e). This affinity is significantly higher than that measured for tracers based on Hsp70s (FITC-Ahx-IEEVD; pKd of 6.8 ± 0.1) or Hsp90s (FITC-Ahx-MEEVD; pKd of 6.1 ± 0.1). An alanine scan of the CHIPOpt sequence in competitive FP experiments established that the positional hierarchy of binding contributions was P2>P1>P4>P5>P3 based on perturbations to the pKi of the peptide (Fig 1f and Supplementary Fig 3). This data suggests that the determinants of CHIP binding extend well beyond the established I/MEEVD motifs.

CHIPOpt engages distinct interactions with CHIP

To better understand the molecular determinants of CHIP specificity, we solved X-ray crystal structures of the human CHIP TPR domain bound to acetylated 5mer peptides corresponding to the Hsp70 sequence (Ac-IEEVD, PDB 6EFK) and CHIPOpt (Ac-LWWPD, PDB 6NSV) at 1.5Å and 1.3Å respectively (Fig 2a, Supplementary Fig 4a, b, Supplementary Table 1). It is worth noting that the CHIPOpt structure included density at the crystallographic interface of the two peptide-bound TPR domains in the asymmetric unit,

which is not present in the Hsp70 peptide-bound structure (Supplementary Fig 4c). This density appeared as a linear chain that wrapped around the epsilon nitrogen of Lys72 in each TPR domain. Given this typical host-guest orientation and the presence of polyethylene glycol (PEG) in the crystallization conditions we modeled the densities as two PEG-6 molecules.

As mentioned above, CHIP belongs to a family of proteins that use TPR domains to bind Hsp70 and Hsp90 C-termini. However, CHIP's TPR domain is unique among these proteins because it contains a discrete hydrophobic pocket formed by an extra turn in helix 6 and an elongated linker between helices 6 and 7, which orient residues Phe98, Phe131 and Ile135 around P5 in the bound peptides (Fig 2b, Supplementary Fig 4d). This arrangement favors a kinked conformation of bound peptides, which contrasts with the linear arrangement of similar peptides in the TPR domain of HOP (Supplementary Fig 4e)[27]. Consistent with this idea, we found that both Hsp70-derived peptide and CHIPOpt peptide had the expected kinked binding mode. A closer examination of the relative orientation of these peptides helped explain why CHIPOpt was a superior ligand. To further that effort, we also performed a computational analysis of the bound peptide in Rosetta[28]. Briefly, using the Hsp70-bound structure as a template, we computationally estimated perturbations to the free energy of folding ($\Delta\Delta G_{fold}$) for the protein-peptide complex upon saturation mutagenesis of the peptide. By this analysis, the amino acids that provided the greatest increases in affinity, such as P4 aromatics and P2 proline, agreed between the experimental results and computational predictions (Supplementary Table 2). Moreover, direct comparison of the P2 position in the Hsp70 and CHIPOpt crystal structures revealed a +19° perturbation to the Φ dihedral angle, suggesting that the conformational rigidity of the proline may enhance favorable contacts elsewhere in the ligand and reduce the entropic cost of binding (Fig 2c, P2-V & P2-P). We also observed that the P4 Trp of CHIPOpt packs on a hydrophobic shelf formed by F98 and F99, which is not engaged by the corresponding P4 Glu in the Hsp70-bound structure. Given that F99 bridges the P4 and P5 binding sites, it is likely that the P4 aromatic also further reinforces the kinked peptide binding mode (Fig 2c, P4-E & P4-W) Another striking difference between the Hsp70 and CHIPOpt structures is an apparent shift in hydrogen bonding at the peptide N-terminus. In our Hsp70 structure and all published CHIP-peptide co-crystal structures, D134 in the TPR domain forms a hydrogen bond with the amide nitrogen of the P5 amino acid (Fig 2d, grey). However, in the CHIPOpt structure, this hydrogen bond does not form. Instead, the amide oxygen of the acetyl group forms a hydrogen bond with K95 (Fig 2d, yellow). This shift seems to support an exaggerated kink in the CHIPOpt conformation. In total, the structural and computational data suggests that the enhanced affinity of CHIPOpt likely arises from optimized interactions at P2, P4 and the N-terminus. Together, these results indicate that previously unknown, high-affinity interactions with CHIP exist within the human proteome.

Proteome-wide prediction of CHIP interactions

We next used the expanded specificity of the CHIP TPR domain to generate an algorithm for predicting peptide sequences that would bind to CHIP (termed CHIPScore). Briefly, PSSCL data from the DSF dataset were normalized to the peptide pool with the highest signal (P2 Pro) (Supplementary Fig 5a). Then, each value for an amino acid at a given position was

summed so that a CHIPScore is equal to the sum of the normalized values for P5, P4, P3 and P2 (Fig 3a). To validate the scoring function, we compared the CHIPScore to the measured pK_i values of the CHIPOpt peptide and its variants as well as Hsp70 and Hsp90 sequences. In this analysis, CHIPScore correlated well with the experimental pK_i values ($R^2 = 0.86$) (Fig 3b). Then, we used CHIPScore to search for binders in the human proteome. First, of the 20,246 protein sequences in the reference proteome, we found that 973 have a C-terminal Asp residue. Among these, only cytosolic Hsp70s and Hsp90s terminate in the canonical (I/M)EEVD motif. However, using CHIPScore, we found an additional eight predicted interactions whose: (i) score exceeded Hsp90 (MEEVD CHIPScore = 1.79) and (ii) were expressed in the cytosol or nucleus (Fig 3c, Supplementary Fig 5b, Supplementary Table 3). Two proteins on this list (NADE and TXLNG) had previously been identified in proteomic studies as potential CHIP binders (Taipale *et al.*), supporting the predictive power of the scoring function.

This finding suggested that only a small number of possible interactions could be identified in the intact C-terminome. However, taking inspiration from the central role of proteolysis in revealing N-termini, we expanded our search space to include latent C-termini that are only unmasked by the activity of proteases. Here, “latent” is used to describe a new C-terminus that can be produced by proteolytic activity. Of the human proteases with well-annotated specificity, the caspase family of cysteine proteases was of particular interest because they exhibit a strong preference for Asp at the P1 position, such that their activity yields a new C-terminus ending in this residue[29,30]. Moreover, extensive experimental and bioinformatic efforts have been previously undertaken to identify and predict caspase substrates. Specifically, 1651 unique P1 Asp caspase cleavage sites have been experimentally validated by N-terminomics[31]. When we searched this dataset with CHIPScore, we identified 84 C-termini that are likely to bind better than Hsp90 to CHIP (Supplementary Fig 5c, Supplementary Table 4). Encouraged by these results, we expanded the search to include a proteome-wide dataset of predicted caspase cleavage sites, which were generated from a support vector machine (SVM) scoring function[32]. To set a threshold SVM score, we compared the distribution of 493,321 proteome-derived SVM scores to the 1,651 experimentally validated caspase cleavage sites and set a cutoff that would include 75% of the validated sites (SVM=−0.464) (Supplementary Fig 5d, e). This process yielded 2,757 candidates with latent C-termini that are predicted to be high affinity ligands for CHIP (Fig 3d, Supplementary Fig 5f, Supplementary Table 5). We anticipate that this list includes many new PPIs between CHIP and caspase substrates, perhaps providing a rich source of regulatory interactions.

To validate a subset of this data, we curated the lists of predicted candidates from the explicit and latent C-terminome datasets. This process directed our attention to tau (cleaved at Asp421; tau^{D421}) and an auto-proteolytic activation site of the inter-domain linker in the caspase-6 zymogen (cleaved at Asp179; caspase-6^{D179})[33]. These sites were of interest because tau^{D421} and caspase-6^{D179} have both been shown to accumulate in the brains of AD patients[34–36]. However, the mechanism underlying the accumulation of these specific fragments has been unclear. Moreover, CHIP had previously been linked to the clearance of tau^{D421} in cellular and animal models[37–39]. Thus, we considered a model in which CHIP might serve as a key regulator of both tau homeostasis and caspase-6 activity through

recognition of latent C-termini in each protein. Before proceeding, we confirmed that peptides based on tau^{D421} and caspase-6^{D179} indeed bound (pIC_{50} values 7.1 ± 0.1 and 5.9 ± 0.1 respectively) to CHIP's TPR domain using competitive FP experiments (Fig 3e and Supplementary Fig 5g).

Caspase cleavage of tau at D^{421} recruits CHIP

In healthy neurons, tau binds to microtubules through its microtubule binding repeats (MBRs)[40]. However, in AD, tau is known to dissociate from microtubules to form neurofibrillary tangles (NFTs)[41]. In the NFTs, tau is often post-translationally modified, including by proteolytic cleavage[42]. Specifically, tau contains a number of validated caspase cleavage sites that accumulate during disease progression (Fig 4a)[43]. Our CHIPScore predictions suggested that the D421 site, in particular, would create a high affinity CHIP-binding site. To explore this idea, we first determined whether CHIP selectively bound the tau^{D421} epitope over others. Using competitive FP experiments, we screened peptides corresponding to the reported caspase cleavage sites, establishing that only the peptide from tau^{D421} interacts with CHIP (Supplementary Fig 6a). To validate binding in the context of a full-length protein, we expressed and purified the 0N4R splice isoform of tau (tau^{FL}) that is expressed in adult neurons, as well as the corresponding tau^{D421} truncation. We found that only tau^{D421}, and not tau^{FL}, could bind to CHIP (pIC_{50} of 6.2 ± 0.03); (Fig 4b). This specificity was confirmed using synthetic FP tracers corresponding to the ten amino acids at the C-terminus of tau^{FL} and tau^{D421} (Supplementary Fig 6b). Independent analyses by DSF corroborated the selectivity for cleaved tau (Supplementary Fig 6c,d) in the context of full-length protein. Multiple caspases have been implicated in tau processing during AD. To determine which ones might produce the tau^{D421} epitope, we created a corresponding 10 amino acid fluorogenic substrate (see Methods) and monitored its cleavage in the presence of a commercially-available panel of active caspase enzymes. This experiment showed that caspase-3 had the most specific activity for the site in the conditions tested, although caspases-1, −6 and −7 also had activity (Supplementary Fig 6e). Indeed, the addition of active caspase-3 (at t = 0) was able to convert tau^{FL} into a CHIP-binding species in a kinetic FP assay (Supplementary Fig 6f). Next, we wondered whether the direct interaction of CHIP with tau^{D421} might promote ubiquitination *in vitro*. These studies showed that tau^{D421}, but not tau^{FL}, was rapidly (~3 min) poly-ubiquitinated by CHIP in the presence of an E2/E1/Ub/ATP mixture. Use of CHIP^{K30A}, a mutation in the carboxylate clamp, significantly reduced the ubiquitination of tau^{D421} (Fig 4c), confirming that the interaction required binding to the TPR domain. This robust ubiquitination was also observed for tau^{FL} processed by caspase-3 *in situ* to generate tau^{D421} (Supplementary Fig 6g). Thus, when tau^{D421} is produced by caspase activity, it directly binds to the CHIP TPR domain and the protein can be poly-ubiquitinated.

To validate the CHIP-tau^{D421} interaction in a cellular context, we generated stable cell lines expressing a doxycycline inducible GFP-0N4R construct terminating in either the tau^{FL} sequence, the tau^{D421} truncation, or tau^{D421A}. Live-cell fluorescence microscopy confirmed that all three proteins were properly associated with cytoskeletal structures consistent with microtubules (Fig 4d). Also, microtubule fractionation showed that each of them was associated with the insoluble pool (Fig 4e). In the absence of tau expression, endogenous

CHIP was present in the soluble fraction in all three cell lines (lanes 1,3,5). This localization was unperturbed by the expression of either tau^{FL} or tau^{D421A} (lanes 2,6). However, induced expression of GFP-tau^{D421} (lane 4) dramatically partitions CHIP to the insoluble, microtubule fraction. These results suggest that CHIP tightly and specifically associates with tau^{D421} in a cellular context.

CHIP specifically inhibits mature caspase-6^{D179}

Active caspase-3, −7 and −9 are inhibited by the E3 ubiquitin ligase XIAP; however, an equivalent endogenous inhibitor for caspase-6 is not known[44]. Caspase-6 undergoes a maturation process similar to caspase-3 and caspase-7 wherein the cleavage of the pro-domain and inter-subunit linker yield the mature, fully activated enzyme. The fully mature enzyme bears the predicted CHIP binding site, caspase-6^{D179}, at the C-terminus of the large subunit (Fig 5a). To understand whether CHIP might act as an endogenous caspase-6 inhibitor, we expressed and purified active enzyme as two polypeptide chains with the large subunit terminating at Asp179 and the small subunit terminating with a 6His tag. Competition binding experiments confirmed that active caspase-6^{D179} binds to CHIP (pIC_{50} = 6.6 ± 0.08) (Fig 5b). The specificity of this interaction to C-terminal recognition was confirmed using biolayer interferometry (BLI) and comparing immobilized CHIP to $CHIP^{K30A}$ (Supplementary Fig 7a). We predicted that CHIP would poly-ubiquitinate caspase-6^{D179} *in vitro*, as was observed for tau^{D421}. However, similar experiments showed that active caspase-6^{D179} was not robustly ubiquitinated under these conditions (Supplementary Fig 7b). However, we found that CHIP acted as an inhibitor of caspase-6^{D179} substrate hydrolysis. Specifically, we used proteolysis of a fluorogenic peptide substrate (Ac-VEID-AMC) to monitor caspase-6^{D179} activity in the presence of CHIP. A kinetic analysis demonstrated potent inhibition of substrate turnover and a mode of action consistent with competitive inhibition (an increase in K_m) (Fig 5c). No significant inhibition was detected with the addition of a $CHIP^{K30A}$ (Supplementary Fig 7c). Thus, CHIP inhibits caspase-6 function, but through a mechanism distinct from XIAP regulation of other caspases.

To determine whether CHIP binds mature caspase-6 in a cellular context, we first generated active caspase-6 in Jurkat cells by treating them with staurosporine (1μM) for two hours. Control and staurosporine treated cell lysates were supplemented with recombinant biotinylated CHIP or biotinylated $CHIP^{K30A}$. Bound proteins were enriched on streptavidin coated magnetic beads, washed, and eluted. We used antibodies specific for caspase-6^{D179} (e.g. active) or caspase-6^{FL} (e.g. inactive) to perform Western blot analyses on cell lysates and eluates from pulldowns. We found that caspase-6^{FL} was depleted upon treatment with staurosporine and that neither CHIP or $CHIP^{K30A}$ were capable of pulling it down (Fig 5d, left panel). Conversely, active caspase-6^{D179} was specifically enriched by pulled-down with CHIP but not $CHIP^{K30A}$ (Fig 5d, right panel). These experiments demonstrate that the CHIP-caspase-6 interaction is dependent on the maturation of the enzyme and integrity of the CHIP TPR carboxylate clamp.

CHIP loss coincides with neoepitope accumulation in AD

These results suggest a molecular mechanism to explain why tau^{D421} and active caspase-6^{D179} accumulate in neurons during AD progression. Specifically, we hypothesized that CHIP levels or function might be diminished during disease progression, contributing to increases in active caspase-6^{D179} and failure to clear tau^{D421} (Fig 6a). To test this idea, we developed a multiplexed fluorescent immunostaining method to interrogate the levels of tau^{D421}, active caspase-6^{D179}, and CHIP in the hippocampus of fixed human tissue from donors with AD pathology in early, middle and late stages of the disease (Braak I, III, and VI, respectively). Briefly, Braak staging characterizes the spread of neurofibrillary tangles across cortical regions and is widely used to stage AD pathology[45]. Consistent with the literature, we found that hippocampal Braak VI tissue exhibited the most significant accumulation of tau^{D421} and active caspase-6^{D179}. In addition, we observed a striking loss in CHIP expression in Braak III and VI (Fig 6b). Analysis of RNAseq data from the Allen Brain Atlas revealed that CHIP mRNA does not significantly change as a function of Braak stage, ApoE status, or age (Supplementary Fig 8a, b and c)[46], suggesting that the observed loss of CHIP at Braak III and VI occurs post transcriptionally. Together, these findings support a model in which loss of CHIP expression allows accumulation of tau^{D421} and potentiates the activity of caspase-6, contributing to the accumulation of both C-termini in AD.

Discussion

Proteostasis mechanisms that act on protein termini, such as the N-End Rule pathways, are fundamentally important in sculpting the proteome. The work described here identifies a C-terminal recognition process that recruits CHIP to sites of caspase cleavage. By determining the specificity of CHIP's TPR domain, we identified ~2,700 latent C-termini that are predicted to be regulated by this protein. Further work is needed to probe the scope and specific roles of these interactions; however, as an initial proof-of-principle, we were drawn to the observation that both tau^{D421} and caspase-6^{D179} were putative CHIP ligands. These proteins had been linked to AD and to each other, yet it was not clear how or if they might be co-regulated and what this might mean for the disease. Indeed, we found that CHIP binds both tau^{D421} and caspase-6^{D179}, directing the ubiquitination of tau^{D421} and inhibiting caspase activity in a ubiquitin-independent way. Both interactions were of high affinity and could be readily observed in cell-based models. Linking these observations together, histopathology studies in AD brains suggested that loss of CHIP could be a contributor to the accumulation of these latent C-termini in advanced disease. Thus, these findings may generate new ideas for the treatment of AD. Given the clinical failures in this therapeutic area, new targets and mechanisms are of utmost importance.

It is worth noting that the identification of CHIP as an endogenous inhibitor of caspase-6 fits well into existing paradigms of caspase signaling. Caspase activity in a cell is limited at multiple levels[47]. However, among the broader caspase family, the regulation of caspase-6 is less understood. Like the other executioner caspases, caspase-6 is capable of auto-activation and exists as a constitutive homodimer[48]. However caspase-6 is insensitive to XIAP and it has a unique attributes that separate it from the other caspases[49,50]. Thus, our finding that

CHIP inhibits caspase-6 suggests a novel mechanism of caspase regulation and fills a gap in the regulatory framework of these important signaling proteases.

Finally, CHIP was previously thought to act primarily (or even exclusively) as a co-chaperone for cytosolic Hsp70/Hsp90. Our work shows that, in some cases CHIP circumvents the requirement for chaperone and binds directly to protein targets. We found that few C-termini within explicit open reading frames (ORFs) are likely to compete with the Hsp70/Hsp90 interaction, but that caspase cleavage created a large number of possible binding events at latent C-termini. We used minimal affinity cut-off values based on the CHIP-Hsp90 interaction, such that the predicted contacts might be expected to compete with the canonical chaperone-dependent roles. However, given the abundance of chaperones in cells, more work will be needed to understand which of these putative contacts displace chaperones from CHIP. An additional complexity is the roles of the other TPR co-chaperones, such as FKBP51 and PPP5C, which also converge on the shared (I/M)EEVD motifs. It seems likely that caspase activity could broadly remodel chaperone and non-chaperone PPIs, creating new opportunities to rapidly and post-translationally regulate critical signaling nodes in cells.

Methods

Protein Purification

Unless otherwise stated all proteins were produced in *E. coli* BL21(DE3) and stored at −80° C. **CHIP and CHIP K30A** (human, His-tagged) were expressed from a pET151 construct with a N-terminal TEV-cleavable 6His Tag. *E. coli* were grown in terrific broth (TB) at 37 °C, induced with 500 μM IPTG in log phase, cooled to 18° C and grown overnight. Cells were harvested, resuspended in binding buffer (50 mM Tris pH 8.0, 10 mM imidazole, and 500 mM NaCl) supplemented with protease inhibitors, sonicated, clarified, and supernatant was applied to Ni-NTA His-Bind Resin (Novagen). Resin was washed with binding buffer and His wash buffer (50 mM Tris pH 8.0, 30 mM imidazole, and 300 mM NaCl). Protein was eluted from the resin with His elution buffer (50 mM Tris pH 8.0, 300 mM imidazole, and 300 mM NaCl). N-terminal His tag was removed by overnight dialysis with TEV protease at 4° C. Digested material was applied to His-Bind resin to remove cleaved His tag, undigested material, and TEV protease. Protein was further purified by size exclusion chromatography (Superdex 200) in 50 mM HEPES pH 7.4, 10 mM NaCl.

CHIP TPR Domain (human, AA 22–154, His-tagged) was expressed from a pMCSG7 construct with an N-terminal TEV-cleavable 6His tag. *E. coli* were grown in TB at 37 °C, induced with 1mM IPTG in log phase, cooled to 24° C and grown overnight. Ni-NTA purification and tag removal were conducted as for FL CHIP. Protein was further purified on a Mono S cation exchange column and stored in 10 mM Tris pH 8.0, 150 mM NaCl, and 2 mM DTT.

0N4R tau^{FL} and 0N4R tau^{D421} (human) were expressed from a pET28 construct. *E. coli* were grown in TB at 37° C. NaCl (500 mM) and betaine (10 mM) were added to media prior to log phase induction with 200 μM IPTG for 3.5 h at 30 °C. Cells were harvested, lysed by microfluidizer, and lysate was boiled for 20 min. Clarified lysate was dialyzed into 20 mM

MES, pH 6.8, 50 mM NaCl, 1 mM EGTA, 1 mM MgCl, 2 mM DTT, 0.1 mM PMSF and purified by cation exchange.

Caspase-6^{D179}(human, His-tag) Large subunit (AA 31–179) and small subunit (AA 194–293, 6XHis) in pET24b (+) and pET23b (+) vectors were co-transformed into Rosetta BL2 (DE3) cells. *E. coli* were grown in 2XYT medium at 37° C, and induced in log phase with 0.2 mM IPTG for 20 h at 16 °C. Cells were harvested, resuspended in 100 mM Tris, pH 8.0, 100 mM NaCl, and lysed by microfluidizer. Supernatant was loaded to Ni- NTA His-Bind Resin for 1 h at 4° C. Resin was washed 2X with 100 mM Tris, pH 8.0, 100 mM NaCl, and 1X with 100 mM Tris, pH 8.0, 100 mM NaCl 40 mM imidazole. Protein was eluted with 50 mL 100 mM Tris, pH 8.0, 100 mM NaCl 200 mM imidazole. Further purification was achieved by anion exchange over a linear gradient of 0 – 1 M NaCl in 20 mM Tris pH 8.0.

UbcH5c (human) was expressed from a pET2 construct. *E. coli* were grown in TB at 37° C and induced in log phase with 500 μM IPTG overnight at 16 °C. Cells were harvested, washed with PBS, and resuspended in 30 mM MES pH 6.0, 1 μM DTT, 1 μg/mL Leupeptin, 1 μg/mL Aprotinin and 1 mM PSMF, sonicated and clarified. Purification was achieved by cation exchange chromatography (SP Sepharose) followed by size exclusion chromatography (Superdex 200) in 50mM Tris, 50 mM KCl, pH 8.0.

Ube1 (human, His-tagged) was expressed from a pET21d construct. *E. coli* were grown in TB at 37° C and induced in log phase with 500 μM IPTG overnight at 16 °C. Cells were harvested, washed with PBS, and resuspended in 50 mM Tris, 150 mM NaCl, 1 mM EDTA-NaOH, pH 8.0, 1 mM DTT, 0.1% (w/v) Triton X-100, 1 mM PSMF, 1 protease inhibitor tablet and sonicated. The soluble fraction was loaded onto Ni-NTA His-Bind Resin for 2 h at 4 °C, washed with 50 mM sodium phosphate pH 8.0 150 mM NaCl and eluted in 50 mM sodium phosphate pH 8.0, 150 mM NaCl, 100 mM imidazole. Further purification was achieved by anion exchange chromatography in 10 mM Tris pH 8.0, 1 mM EDTA, 1 mM DTT and size exclusion chromatography (Superdex 200) in 20 mM Tris pH 8.0, 100 mM NaCl, 1 mM EDTA, 1 mM DTT.

Ubiquitin (human) was expressed from a pET15 construct. *E. coli* were grown in TB at 37° C and induced in log phase with 500 μM IPTG overnight at 16 °C. Cells were harvested, washed with PBS, resuspended in Lysis buffer (50 mM Tris, 1mM EDTA pH 7.6 + 0.05% Tween-20) and sonicated. The soluble fraction was dialyzed twice into 3.5 L 50 mM sodium acetate pH 4.5. Dialyzed sample was pelleted by centrifugation at 18,000 RPM for 20 min. Supernatant was loaded onto a cation exchange column (SP Sepharose) and eluted in 50 mM sodium phosphate pH 4.5 and NaCl. Fractions containing ubiquitin were purified further by SEC (Superdex 75) in 50 mM Tris pH 8.0, 50 mM KCl.

Protein modification with maleimide-biotin or maleimide-FAM—Tau and CHIP were dialyzed into 25 mM HEPES pH 7.4 50 mM KCl, 1 mM TCEP and labeled with 1.1 eq of maleimide-biotin or maleimide-FAM for 1 h at room temperature. Caspase-6 was labeled with 2 eq maleimide-FAM overnight at 4° C in purification buffer supplemented with 1 mM TCEP. Excess reagent was removed by iterative dilution and concentration.

Peptide Synthesis

Peptides were synthesized by Fmoc solid phase peptide synthesis on a Syro II peptide synthesizer (Biotage) at ambient temperature and atmosphere on a 12.5 μmol scale using pre-loaded Wang resin. Coupling reactions were conducted with 4.9 eq of HCTU (O-(1H-6-Chlorobenzotriazole-1-yl)-1,1,3,3-tetramethyluronium hexafluoro-phosphate), 5 eq of Fmoc-AA-OH and 20 eq of N-methylmorpholine (NMM) in 500 uL of N,N dimethyl formamide (DMF). Reactions were run for 8 min while shaking. Each position was double coupled. Fmoc deprotection was conducted with 500 uL 40% 4-methypiperadine in DMF for 3 minutes, followed by 500 μL 20% 4-methypiperadine in DMF for 10 minutes, and six washes with 500 μL of DMF for three minutes. Acetylation was achieved by reaction with 20 eq acetic anhydride and 20 eq NMM in 500 μL DMF for 1 h while shaking. Peptides were cleaved with 500 μL of cleavage solution (95% Trifluoroacetic acid 2.5% Water 2.5% Triisoprpylsilane) while shaking for 1 h. Crudes were precipitated in 10 mL cold 1:1 diethyl ether : hexanes. Peptide crudes were solubilized in a 1:1:1 mixture DMSO: water: acetonitrile and purified by HPLC on a Agilent Pursuit 5 C18 column (5 mm bead size, 150 mm × 21.2 mm) using an Agilent PrepStar 218 series preparative HPLC. The mobile phase consisted of A: Water 0.1% Trifluoroacetic acid and B: Acetonitrile 0.1% Trifluoroacetic acetic acid. Solvent was removed under reduced atmosphere and 10 mM DMSO stocks were made based on the gross peptide mass. Purity was confirmed by LC/MS. Stocks were stored at −20 °C. Fluorescein isothiocyanate (FITC) was added to FP tracers by reacting 1.7 eq of FITC and 20 eq of NMM in 500 uL of DMF for while shaking for 1 h. FITC capping reactions were run twice. The quenched fluorogenic peptide corresponding to the tau^{D421} site (NH_2-K(MCA)IDMVD/SPQLAK(DNP)-COOH) was synthesized as above where fluorophore (7-Methoxycoumarin-4-acetic acid (MCA)) and the quencher (2,4-dinitrophenyl (DNP)) are linked to the epsilon nitrogen of a lysine. Peptide was synthesized using Wang resin pre-loaded with Fmoc-Lys(DNP)-OH (Millipore). Fmoc-Lys(MCA)-OH coupling reactions were conducted with 1.7 eq monomer and HCTU.

The PSSCL library was synthesized using standard coupling conditions outlined above. “Mixed” positions in the library were coupled with an equimolar mixture of all twenty proteinogenic Fmoc protected amino acid monomers. Pools were cleaved and used without further purification. Molecular weights were estimated by using 110 Da (the average MW of a natural amino acid) for mixed positions.

DSF

PSSCL screens were conducted in a 96-well qRT-PCR plate on a Strategene Mx3005P-rtPCR. Each well contained 10 μL 10 μM CHIP in in 25 mM HEPES pH 7.4 50 mM KCl 1 mM TCEP, 10 μL of 200 μM PSSCL pool in the same buffer + 0.2% CHAPS + 2% DMSO, and 5 μL 25X Sypro Orange dye. Fluorescence intensity readings were taken over 70 cycles where reactions were heated to desired temp and then cooled to 25° C before reading. Temperature was increased at a rate of 1° C per cycle. Fluorescence Intensity data was normalized and truncated at 55° C to fit to a Boltzmann Sigmoid in Graphpad Prism 7.0.

$$Y = Bottom + ((Top - Bottom)/(1 + \exp(T_m - T/Slope)) \quad (1)$$

Binding to CHIP was assessed by the change in T_m.

$$\Delta T_m = \Delta T_{POOL} - \Delta T_{DMSO} \quad (2)$$

Tau DSF was conducted as above with 10 μL of 10 μM (1eq) tau in lieu of the peptide library.

FP Binding Assay

FP assays were run in 18 μL in a Corning black 384 well round bottom low volume plate and read on a BioTek H4 multimode plate reader at 21° C.

PSSCL screens were performed by measuring displacement of CHIP tracers corresponding to the Hsc70 or Hsp90a sequences (FAM-Ahx-SSGPTIEEVD and FAM-Ahx-DDTSRMEEVD). 2X Protein-tracer complexes (20 nM Tracer +2X EC_{85} CHIP) were prepared in 25 mM HEPES pH 7.4 50 mM KCl 1 mM TCEP. 2X (200 μM) PSSCL pool was prepared in the same buffer + .2% CHAPS + 2% DMSO. Each solution was added to the well and incubated for 15 min. ΔPolarization (mP) was calculated relative to DMSO control. Final concentration of CHIP was 1.58 μM for Hsc70 and 3.48 μM for Hsp90α.

Saturation binding assays with 1 nM FITC-CHIPOpt (FITC-Ahx-LWWPD), FITC-Hsp70 (FITC-Ahx-IEEVD), and FITC-Hsp90 (FITC-Ahx-MEEVD) were run in a final buffer composition of 25 mM HEPES pH 7.4, 50 mM KCl, .01% Triton X-100 and 1% DMSO. Raw polarization (mP) data were normalized and plotted relative to $\log_{10}$[CHIP]M. Data was fit to the model for log(agonist) vs response (variable slope) in Graphpad Prism 7.0. K_d was extrapolated from EC_{50}. Tau tracer saturation binding was identical except that 0.1% CHAPS was substituted for .01% Triton X-100 and tracer concentration was 20 nM.

$$Y = Bottom + (Top - Bottom)/(1 + 10\text{^}(LogEC_{50} - X) * HillSlope)) \quad (3)$$

Competition binding assays A 2X stock of CHIP+Tracer was made in HEPES pH 7.4, 50 mM KCl so that the final concentration of protein would be EC_X and tracer would be 1 nM. 2X peptide stock was prepared in 25 mM HEPES pH 7.4 50 mM KCl .02% Triton X-100 and 2% DMSO. Raw polarization (mP) data were plotted relative to $\log_{10}$[Peptide]M. Data was fit to the model for log(antagonist) vs response (variable slope) in Graphpad Prism 7.0.

$$Y = 100/(1 + 10\text{^}((LogIC_{50} - X) * HillSlope))) \quad (4)$$

K_i was calculated form EC_{50}[51].

$$K_i = [I]_{50}/([L]_{50}/K_d+[P]_0/K_d+1) \quad (5)$$

Kinetic FP A 2X stock of CHIP+Tracer (1000 nM CHIP 20 μM FAM-Ahx-SSGPTIEEVD) was prepared in 25 mM HEPES pH 7.4 50mM KCl 1 mM TCEP, 0.1% CHAPS. A 2X stock of tau^{FL} or tau^{D421} (20 μM) was prepared in the same buffer. 9 μL of each 2X stock were added to the wells in triplicate. An initial FP reading was recorded. 2 μL of active caspase-3 (10X or 50nM) in the same assay buffer and added to each well. FP readings were taken every 46 s for 20 min. A well with no tau was included to account for effects of caspase on CHIP binding to tracer.

Competition binding with FL Tau and Caspase-6 were run identically to peptide competition binding experiments with the Hsp70 tracer (FITC-Ahx-IEEVD) but in 50 mM HEPES pH 7.5, 25mM $MgSO_4$, 0.5 mM EGTA, 5 mM reduced glutathione, and .01% Triton X100. Tracer was used at a final concentration of 20 nM.

X-Ray Crystallography

The protein solution was prepared by mixing a 1:1 molar ratio of human CHIP-TPR, at 7 mg/ml, and the 5mer 70 or CHIPOpt peptide in protein buffer (10 mM Tris-HCl pH 8.0, 150 mM NaCl and 2 mM DTT), and incubated on ice for 30 min. Crystals of the complex were grown at room temperature by hanging-drop by mixing 100 nL of the protein solution with 100 μL of the crystallization condition (**Hsp70:** 0.4 M $CaCl_2$, 0.1 M HEPES (pH 7.5), 25% PEG 4K) **CHIPOpt:** 0.05M $CaCl_2$, 0.1 HEPES (pH 7.0), 28% PEG 4K, 0.01M $CoCl_2$) by TTPLabtech Mosquito Nanoliter Dropsetter. Crystals appear within 24 h and were harvested ~ 1 week after setup by flash-freezing in liquid nitrogen using a cryogenic solution of 50% MPD in the crystallization condition. Data were collected at Lawrence Berkeley National Laboratory Advanced Light Source beamline 8.3.1. Diffraction images were processed using Xia2 with the Dials pipeline[52]. Automatic molecular replacement was performed using the online Balbes tool[53]. The resulting structure models were refined over multiple rounds of restrained refinement and isotropic B-factor minimization with Phenix[54]. For 6EFK Ramachandran favored=98.5%, allowed=1.5%, outliers=0%. For 6NSV Ramachandran favored=98.46%, allowed=1.54%, outliers=0%.

Rosetta ΔΔG calculations

The energetics of particular mutations were assessed computationally using ddg_monomer from the Rosetta suite using the solved structure of CHIP TPR bound to Ac-IEEVD peptide as starting model. Structures of starting model and mutants underwent three rounds of energy minimization. Fifty iterations of the ΔΔG optimization process were performed and the model with the lowest overall energy was used for analysis.

Protease Activity Assays

Caspase screening was conducted with a panel of commercially available active caspase −1, −2, −3, −6, −7, −8, −9 and −10 (Enzo Life Sciences, ALK-850–243-KI01). 1 unit of enzyme was added to 10 μM of fluorogenic substrate corresponding to the tau^{D421} cleavage site in 25 mM HEPES pH 7.4 50 mM KCl 0.1% CHAPS 1 mM TCEP. Fluorescence intensity was monitored as a function of time. Enzymes were compared based on the initial velocity of the reaction.

Caspase 6 kinetic assays The activity of a final enzyme concentration of 10 nM was monitored using a fluorogenic substrate (Ac-VEID-AMC). To each well was added a 4X stock of caspase-6^{D179} and a 4X stock of CHIP in 50 mM HEPES pH 7.5, 25 mM $MgSO_4$, 0.5 mM EGTA, 5 mM reduced glutathione, and 0.01% Triton X100. This mixture was incubated at ambient temperature for 10 min. Substrate was added immediately prior to reading as a 2X stock in 50 mM HEPES pH 7.5, 25 mM $MgSO_4$, 0.5 mM EGTA, 5 mM reduced glutathione, and 0.01% Triton X100 +2% DMSO. Activity was monitored at 30 s intervals for 10min. V_0 was calculated from data collected in the interval between 30 s and 360 s in arbitrary units (RFU/s).

Ubiquitination Assays

Four 4X stocks were prepared: (A) Ube1 + UbcH5c (400 nM Ube1 and 4 μM UbcH5c), (B) Ubiquitin (1 mM Ub), (C) ATP + $MgCl_2$ (10 mM ATP and 10 mM $MgCl_2$), and (D) CHIP + substrate (4 μM CHIP and 4 μM FAM-MAPT or FAM-caspase-6) in 50 mM Tris, 50 mM KCl, pH 8.0. Ubiquitination reactions were set up by adding 27.5 μL of each 4X stock, in order from A to D, for a final volume of 110 μL (100 nM Ube1, 1 μMUbcH5c, 250 μM ubiquitin, 2.5 mM ATP, 2.5 mM $MgCl_2$, 1 μM CHIP, 1 μM FAM-substrate). Reactions incubated at room temperature, quenching 10 μL aliquots in 5 μL 3X SDS-PAGE running buffer after the appropriate incubation period. Gel was imaged at Alexa488 channel on Biorad Imager.

Biolayer Interferometry

A qualitative analysis of the selective interaction between CHIP and caspase-6^{D179} was conducted using biolayer interferometry (BLI) on an Octet Red 384well system (ForteBio). Biotinylated CHIP or CHIP K30A were loaded onto a BLI sensor coated with streptavidin. Association was observed by immersing loaded tips into solutions of caspase-6^{D179} at varying concentrations in 50 mM HEPES pH 7.5, 25mM $MgSO_4$, 0.5 mM EGTA, 5 mM reduced glutathione, and 1% BSA for 240 s. Dissociation was observed by transferring the tip of a well with the same buffer and no caspase-6 for 450 s. Relative binding was assessed qualitatively.

SDS PAGE Gels

All SDS PAGE was run on a precast 15will 4–15% gel (Biorad) for 33 min at 200V

Western Blotting

Transfers were conducted on nitrocellulose membranes using a Trans-Blot Turbo Transfer system (Bio-Rad). Membranes were blocked with Odyssey TBS blocking buffer (Licor) for 1h at room temperature. Primary antibodies were diluted 1:2000 in blocking buffer and incubated overnight at 4C. Membranes were washed 5×3min with TBST and probed with secondary for 1h at room temperature. Secondaries were washed 5×3min with TBST and imaged on a Licor Fc imaging system.

Imaging

Cells were seeded in a clear bottom, TC treated 96 well plate at 10K cells/well in 100μL complete growth medium and allowed to adhere overnight. Cells were induced with 10 μg/mL Doxycycline for 72h. Nuclei were counter stained with 1 μg/mL Hoechst 33342 in complete growth media for 30 min before imaging. Live-cell images were taken at 40X magnification on a GE InCell 6000.

Microtubule Pulldowns

Flp-In T-Rx 293 cell lines expressing GFP-0N4R tau constructs were generated, propagated, and stored according to the manufacturer's instructions (https://www.thermofisher.com/order/catalog/product/R78007). 150K cells were seeded in a 6-well plate in 3 mL complete growth medium (DMEM, 10% FBS, 1% Penicillin/Streptomycin), allowed to adhere for 12h, and induced with 10 μg/mL Doxycycline for 72h. Media was removed and cells were washed with DPBS. Cell membranes were lysed with 90 μL of a microtubule-stabilizing lysis buffer (20 mM MOPS pH 6.8, 50 mM NaCL, .5% NP-40, 2 mM EGTA, 1 mM $MgCl_2$, 2 mM TCEP, 2 μg/mL paclitaxel, 2 mM GTP, 250 unit/mL benzonase) and rocked gently for 3 min. Soluble lysate was removed gently with a cut pipette tip. The well was rinsed gently with 45 μL of lysis buffer and the soluble fraction and centrifuged at 15K RPM at room temp. 50 μL of was diluted in 3X SDS-PAGE loading buffer. 200 μL of 1X SDS-PAGE loading buffer was added to the well to solubilize the microtubule fraction. Samples were boiled and 15 μL loaded for Western Blot analysis. Membranes were probed with mouse αGFP (Santa Cruz), mouse αTubulin (Santa Cruz), and Rabbit αCHIP (Abcam). Blots were developed using Licor secondary antibodies (Goat-αRabbit 680RD and Goat-αmouse 800CW).

Biotin-CHIP Pulldowns

Jurkat cells were cultured according to ATCC (RPMI-1640, 10% FBS, 1% Penicillin/Streptomycin). For pull-down experiments cells were seeded at 500K/mL in complete growth media and treated with either 1 μM Staurosporine (from a 1000X DMSO stock) or DMSO alone for 2h. Cells were harvested by centrifugation and washed with DPBS. Washed cell pellets were flash frozen. Cells pellets were thawed and lysed at room temp for 5 min while shaking in 10 μL of M-PER (Thermo-Fischer Scientific) per million cells. 50 μL (5 million cells) of lysate was diluted with 150 μL of TBS pH 8.0. Biotinylated CHIP (WT or K30) was added to the diluted lysate so that the final concentration of CHIP was 1 μM and the mixture was allowed to incubate for 1h. After incubation Biotinylated CHIP was enriched by incubation with 100 μL of streptavidin coated magnetic bead slurry

(MagneSphere, Promega) for 1h at room temperature. Beads were washed 3x with TBS and eluted in 50 μL of 1X loading buffer. 15 μL of eluate was for Western Blot analysis with Licor secondary antibody (Goat αRabbit 800CW).

Brain Immunofluorescence

The de-identified post mortem tissues were sourced from the Brain Bank of the Brazilian Brain Aging Study Group and the Neurodegenerative Disease Brain Bank at UCSF as previously described (https://memory.ucsf.edu/neurodegenerative-disease-brain-bank)[55]. AD was categorized according to the Braak staging system and CERAD neuropathology criteria. All cases represented sporadic AD and included Braak 1 (early AD), Braak 3 (mid-AD), and Braak 6 (late AD). Blocks of the entorhinal cortex-hippocampus were embedded in paraffin and cut in serial sections. To visualize the interaction of different markers and their overlapping positivity, the sections were stained with multiplex immunofluorescence (IF). Sections were autoclaved in citrate buffer retrieval solution at 121 °C. Primary antibodies (aCasp6 from Aviva Scientific, CHIP from Sigma Aldrich and TauC3 from Life Technologies; all 1:200) were incubated overnight, followed by species-specific secondary antibodies for 1 h. Neuronal cell bodies were labeled with Neurotrace 435/455 for 30 min (1:50; Life Tech), a fluorescent Nissl stain. Sections were visualized with a 20x objective (Plan Apo N.A. 0.75, Nikon, Japan) using a Nikon 6D high throughput wide field epifluorescence microscope (Nikon, Tokyo, Japan) at the UCSF Nikon Imaging Center.

Supplementary Material

Refer to Web version on PubMed Central for supplementary material.

Acknowledgments:

This work is dedicated to Ron Raines on the occasion of his 60th birthday. This work was supported by grants from the Tau Consortium and NIH R01059690 (to J.EG), P41CA196276 and P50GM082250 (to C.S.C), K24 AG053435 (to L.T.G.) Alzheimer Association AARG-16–441514 (to L.T.G. and M.A.). Additional support included an NSF GRFP fellowship (to K.A.O), an ARCS Foundation fellowship (to M.R.), institutional grants UL1 TR001872 and K01AG053433 (to P.T.), and a Program for Breakthrough Biomedical Science funded by the Sandler Foundation (to C.S.C.). The authors would like to thank the laboratories of K. Matthew Scaglione (Medical College of Wisconsin) and James A. Wells (University of California San Francisco) for technical support, as well as Sue-Ann Mok for input on the manuscript.

References

1. Dougan DA, Micevski D & Truscott KN The N-end rule pathway: From recognition by N-recognins, to destruction by AAA+proteases. Biochim. Biophys. Acta - Mol. Cell Res 1823, 83–91 (2012).
2. Tonikian R et al. A specificity map for the PDZ domain family. PLoS Biol. 6, 2043–2059 (2008).
3. Dong C et al. Molecular basis of GID4-mediated recognition of degrons for the Pro/N-end rule pathway article. Nat. Chem. Biol 14, 466–473 (2018). [PubMed: 29632410]
4. Zhang C et al. High-resolution crystal structure of human protease-activated receptor 1. Nature 492, 387–92 (2012). [PubMed: 23222541]
5. Saelens X et al. Toxic proteins released from mitochondria in cell death. Oncogene 23, 2861–2874 (2004). [PubMed: 15077149]
6. Ye J et al. ER stress induces cleavage of membrane-bound ATF6 by the same proteases that process SREBPs. Mol. Cell 6, 1355–1364 (2000). [PubMed: 11163209]

7. Zheng N & Shabek N Ubiquitin Ligases : Structure, Function, and Regulation. Annu. Rev. Biochem 86, 129–157 (2017). [PubMed: 28375744]
8. Bachmair A, Finley D & Varshavsky A In vivo half-life of a protein is a function of its amino-terminal residue. Science 234, 179–186 (1986). [PubMed: 3018930]
9. Chen S-J, Wu X, Wadas B, Oh J-H & Varshavsky A An N-end rule pathway that recognizes proline and destroys gluconeogenic enzymes. Science 355, eaal3655 (2017). [PubMed: 28126757]
10. Kim HK et al. The N-terminal methionine of cellular proteins as a degradation signal. Cell 156, 158–169 (2014). [PubMed: 24361105]
11. Varshavsky A The N-end rule pathway and regulation by proteolysis. Protein Sci. 20, 1298–1345 (2011). [PubMed: 21633985]
12. Koren I et al. The Eukaryotic Proteome Is Shaped by E3 Ubiquitin Article The Eukaryotic Proteome Is Shaped by E3 Ubiquitin Ligases Targeting C-Terminal Degrons. Cell 173, 1622–1635.e14 (2018). [PubMed: 29779948]
13. Lin H et al. C-Terminal End-Directed Protein Elimination by CRL2 Ubiquitin Ligases. Mol. Cell 70, 602–613.e3 (2018). [PubMed: 29775578]
14. Scott FL et al. XIAP inhibits caspase-3 and −7 using two binding sites: Evolutionary conserved mechanism of IAPs. EMBO J. 24, 645–655 (2005). [PubMed: 15650747]
15. Saita S et al. PARL mediates Smac proteolytic maturation in mitochondria to promote apoptosis. Nat. Cell Biol 19, 318–328 (2017). [PubMed: 28288130]
16. Wu G et al. Structural basis of IAP recognition by Smac/DIABLO. Nature 408, 1008–1012 (2000). [PubMed: 11140638]
17. Ballinger CA et al. Identification of CHIP, a novel tetratricopeptide repeat-containing protein that interacts with heat shock proteins and negatively regulates chaperone functions. Mol. Cell. Biol 19, 4535–4545 (1999). [PubMed: 10330192]
18. Jiang J et al. CHIP Is a U-box-dependent E3 Ubiquitin Ligase. J. Biol. Chem 276, 42938–42944 (2001). [PubMed: 11557750]
19. Zhang M et al. Chaperoned ubiquitylation - Crystal structures of the CHIP U box E3 ubiquitin ligase and a CHIP-Ubc13-Uev1a complex. Mol. Cell 20, 653–659 (2005). [PubMed: 16337587]
20. Qian SB, McDonough H, Boellmann F, Cyr DM & Patterson C CHIP-mediated stress recovery by sequential ubiquitination of substrates and Hsp70. Nature 440, 551–555 (2006). [PubMed: 16554822]
21. Rodina A et al. The epichaperome is an integrated chaperome network that facilitates tumour survival. Nature 538, 397–401 (2016). [PubMed: 27706135]
22. Taipale M et al. A quantitative chaperone interaction network reveals the architecture of cellular protein homeostasis pathways. Cell 158, 434–448 (2014). [PubMed: 25036637]
23. Wang L et al. Molecular mechanism of the negative regulation of Smad1/5 protein by Carboxyl terminus of Hsc70-interacting Protein (CHIP). J. Biol. Chem 286, 15883–15894 (2011). [PubMed: 21454478]
24. Assimon VA, Southworth DR & Gestwicki JE Specific Binding of Tetratricopeptide Repeat Proteins to Heat Shock Protein 70 (Hsp70) and Heat Shock Protein 90 (Hsp90) Is Regulated by Affinity and Phosphorylation. Biochemistry 54, 7120–7131 (2015). [PubMed: 26565746]
25. Choe Y et al. Substrate profiling of cysteine proteases using a combinatorial peptide library identifies functionally unique specificities. J. Biol. Chem 281, 12824–32 (2006). [PubMed: 16520377]
26. Brinker A et al. Ligand discrimination by TPR domains. Relevance and selectivity of EEVD-recognition in Hsp70·Hop·Hsp90 complexes. J. Biol. Chem 277, 19265–19275 (2002). [PubMed: 11877417]
27. Scheufler C et al. Structure of TPR domain-peptide complexes: Critical elements in the assembly of the Hsp70-Hsp90 multichaperone machine. Cell 101, 199–210 (2000). [PubMed: 10786835]
28. Kellogg EH, Leaver-Fay A & Baker D Role of conformational sampling in computing mutation-induced changes in protein structure and stability. Proteins Struct. Funct. Bioinforma 79, 830–838 (2011).

29. Thornberry NA et al. A novel heterodimeric cysteine protease is required for interleukin-l fJ processing in monocytes. Nature 356, 768–774 (1992). [PubMed: 1574116]
30. Julien O & Wells JA Caspases and their substrates. Cell Death Differ. 24, 1380–1389 (2017). [PubMed: 28498362]
31. Crawford ED et al. The DegraBase: A Database of Proteolysis in Healthy and Apoptotic Human Cells. Mol. Cell. Proteomics 12, 813–824 (2012). [PubMed: 23264352]
32. Barkan DT et al. Prediction of protease substrates using sequence and structure features. Bioinformatics 26, 1714–1722 (2010). [PubMed: 20505003]
33. Stennicke HR & Salvesen GS Caspases - Controlling intracellular signals by protease zymogen activation. Biochim. Biophys. Acta - Protein Struct. Mol. Enzymol 1477, 299–306 (2000).
34. Rissman R. a. et al. Caspase-cleavage of tau is an early event in Alzheimer disease tangle pathology. J. Clin. Invest 114, 121–130 (2004). [PubMed: 15232619]
35. Guo H et al. Active caspase-6 and caspase-6-cleaved tau in neuropil threads, neuritic plaques, and neurofibrillary tangles of Alzheimer's disease. Am. J. Pathol 165, 523–531 (2004). [PubMed: 15277226]
36. Theofilas P et al. Probing the correlation of neuronal loss, neuro fibrillary tangles, and cell death markers across the Alzheimer's disease Braak stages : a quantitative study in humans. Neurobiol. Aging 61, 1–12 (2018). [PubMed: 29031088]
37. Dolan PJ & Johnson GVW A caspase cleaved form of tau is preferentially degraded through the autophagy pathway. J. Biol. Chem 285, 21978–21987 (2010). [PubMed: 20466727]
38. Saidi L-J et al. Carboxy Terminus Heat Shock Protein 70 Interacting Protein Reduces Tau-Associated Degenerative Changes. J. Alzheimer's Dis 44, 937–947 (2015). [PubMed: 25374103]
39. Dickey C. a et al. Deletion of the ubiquitin ligase CHIP leads to the accumulation, but not the aggregation, of both endogenous phospho- and caspase-3-cleaved tau species. J. Neurosci 26, 6985–6996 (2006). [PubMed: 16807328]
40. Kellogg EH et al. Near-atomic model of microtubule-tau interactions. Science 360, 1242–1246 (2018). [PubMed: 29748322]
41. Fitzpatrick AWP et al. Cryo-EM structures of tau filaments from Alzheimer's disease. Nature 547, 185–190 (2017). [PubMed: 28678775]
42. Morris M et al. Tau post-translational modifications in wild-type and human amyloid precursor protein transgenic mice. Nat. Neurosci 18, 1183–1189 (2015). [PubMed: 26192747]
43. Quinn JP, Corbett NJ, Kellett KAB & Hooper NM Tau Proteolysis in the Pathogenesis of Tauopathies: Neurotoxic Fragments and Novel Biomarkers. J. Alzheimer's Dis 63, 1–21 (2018). [PubMed: 29578489]
44. Deveraux QL, Takahashi R, Salvesen GS & Reed JC X-linked IAP is a direct inhibitor of cell-death proteases. Nature 388, 300–304 (1997). [PubMed: 9230442]
45. Braak H, Braak E & Bohl J Staging of alzheimer-related cortical destruction. Eur. Neurol 33, 403–408 (1993). [PubMed: 8307060]
46. J.A. M et al. Neuropathological and transcriptomic characteristics of the aged brain. Elife 6, 1–26 (2017).
47. Riedl SJ & Salvesen GS The apoptosome: signalling platform of cell death. Nat. Rev. Mol. Cell Biol 8, 405–413 (2007). [PubMed: 17377525]
48. Klaiman G, Champagne N & Leblanc AC Self-activation of Caspase-6 in vitro and in vivo : Caspase-6 activation does not induce cell death in HEK293T cells. Biochem Biophys Acta 1793, 592–601 (2009). [PubMed: 19133298]
49. Dagbay KB & Hardy JA Multiple proteolytic events in caspase-6 self-activation impact conformations of discrete structural regions. Proc. Natl. Acad. Sci 114, E7977–E7986 (2017). [PubMed: 28864531]
50. Julien O et al. Quantitative MS-based enzymology of caspases reveals distinct protein substrate specificities, hierarchies, and cellular roles. Proc. Natl. Acad. Sci. U. S. A 113, E2001–10 (2016). [PubMed: 27006500]

51. Nikolovska-Coleska Z et al., Development and optimization of a binding assay for the XIAP BIR3 domain using fluorescence polarization. Anal. Biochem 332, 261–273 (2004). [PubMed: 15325294]

52. Winter G, Xia2: An expert system for macromolecular crystallography data reduction. J. Appl. Crystallogr 43, 186–190 (2010).

53. Long F, Vagin AA, Young P, Murshudov GN, BALBES: A molecular-replacement pipeline. Acta Crystallogr. Sect. D Biol. Crystallogr 64, 125–132 (2007). [PubMed: 18094476]

54. Adams PD et al., PHENIX: A comprehensive Python-based system for macromolecular structure solution. Acta Crystallogr. Sect. D Biol. Crystallogr 66, 213–221 (2010). [PubMed: 20124702]

55. Grinberg LT et al. Brain bank of the Brazilian aging brain study group - A milestone reached and more than 1,600 collected brains. Cell Tissue Bank. (2007). 8, 151–162 [PubMed: 17075689]

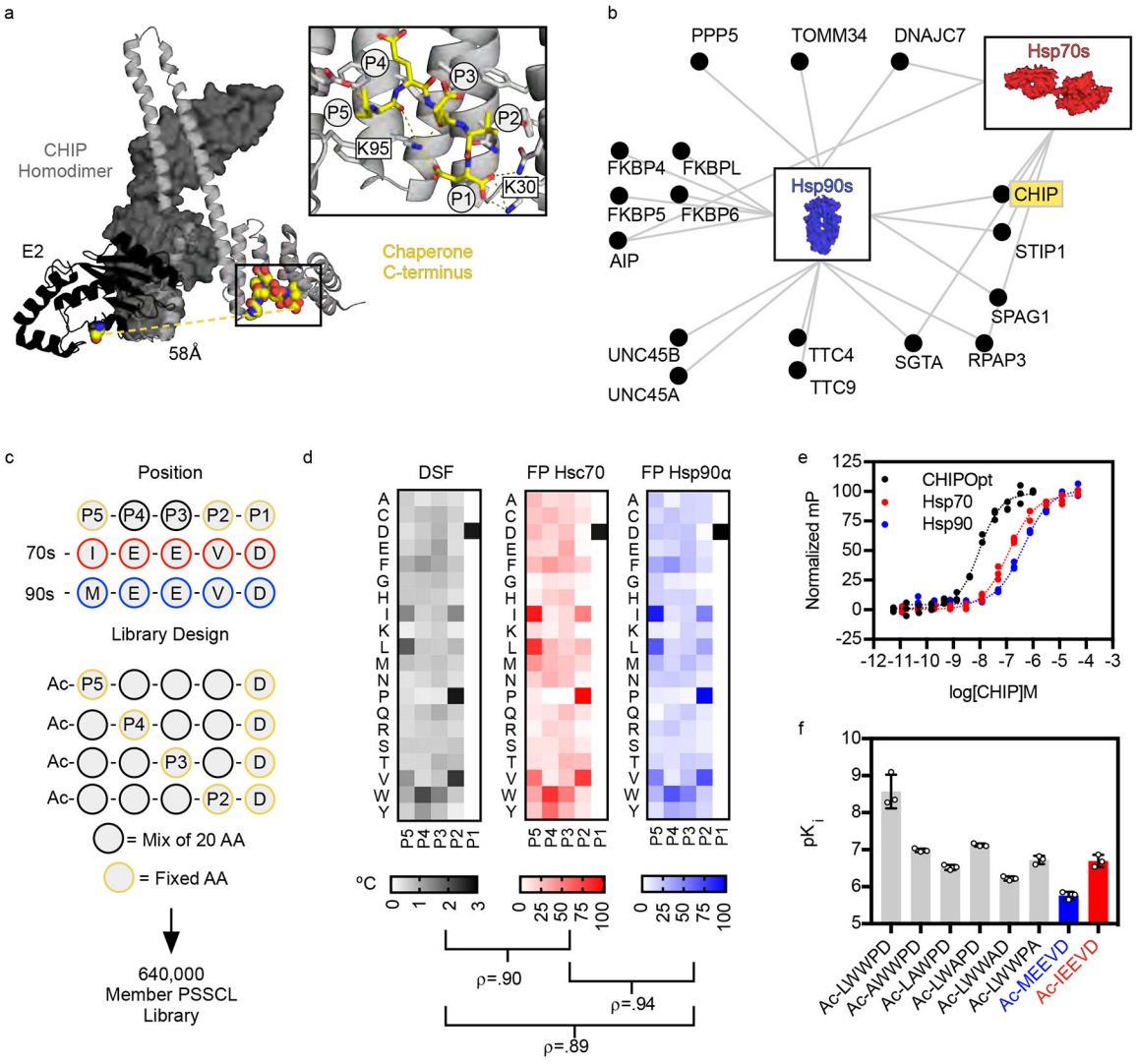

Fig. 1. CHIP function is rooted in the recognition of C-termini.

a, A composite structural model depicting how the CHIP homodimer (grey surface/cartoon) positions the E2 ubiquitin conjugating enzyme UBCH5 (black cartoon) so that the chaperone tail is 58Å away from the activated ubiquitin thioester (yellow spheres) (PDB: 2C2L and 2OXQ). The critical motif for chaperone binding to CHIP spans the last five amino acids (P5,4,3,2,1, yellow) of Hsp70s and Hsp90s (PDB: 3Q49). **b,** Lines represent experimentally validated interactions between cytosolic Hsp70 (red) or Hsp90 (blue) chaperones with TPR co-chaperones (black circles). CHIP (yellow) is the only E3 ubiquitin ligase amongst these TPR co-chaperones. **c,** The terminal sequences of Hsp70s (red) and 90s (blue) bind to CHIP's TPR domain. Positions P5, P2, and P1 (yellow) are critical for binding. A PSSCL library was designed to sample amino acid diversity at P5, P4, P3 and P2. **d,** Each peptide pool was analyzed by DSF and two competitive fluorescence polarization (FP) assays, yielding $\Delta(T_m)$ and Δ(mP) values. Pearson's *r* was used to compare the data sets to one another. These experiments indicated that affinity is not optimized in the natural peptides (IEEVD or MEEVD). **e,** A saturation FP experiment with tracers corresponding to

the optimized sequence “CHIPOpt” (FITC-Ahx-LWWPD, black), Hsp70 (FITC-Ahx-IEEVD, red), and Hsp90 (FITC-Ahx-MEEVD, blue). Normalized polarization is plotted for individual replicate samples (n=3) in a representative experiment. Reported pK_d is a mean of pK_d values from independent experiments (n=3) with error reported as SEM. **f,** Competition binding FP experiments with an alanine scanning library of CHIPOpt. pK_i values calculated from independent experiments (n=3) are plotted individually (open circles). Bars represent mean pK_i. Error is plotted as SEM.

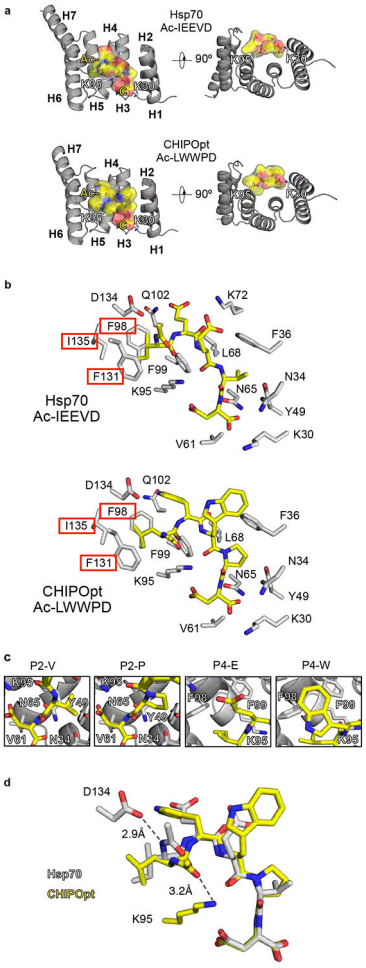

Fig. 2. Structural basis for CHIP TPR domain specificity.

a, X-ray crystal structures of Hsp70 peptide (PDB ID 6EFK) or CHIPOpt peptide (PDB ID 6NSV) bound to CHIP's TPR domain were solved at 1.5 and 1.3 Å respectively. **b,** The overall binding mode is conserved between Hsp70 and CHIPOpt peptides. **c,** At the P2 position the proline in CHIPOpt fixes the Φ at −67.5° vs −86.4 for the P2 valine in Hsp70. The P4 tryptophan in CHIPOpt occupies a hydrophobic shelf formed by F98, F99, and L68. **d,** A kinked backbone orientation supports hydrogen bonding between the acetyl oxygen and K95 in the carboxylate clamp by CHIPOpt (yellow) rather than the acetyl nitrogen and D134 in Hsp70 (grey).

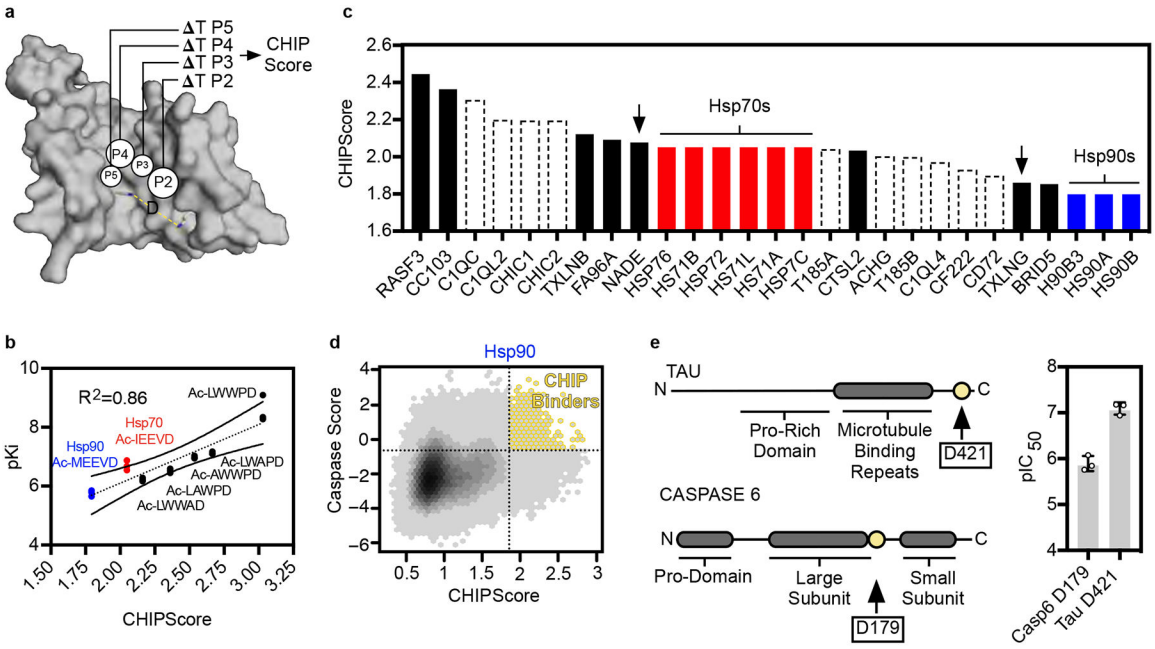

Fig. 3. Proteome-wide prediction of CHIP TPR interactions with C-termini.

a, A model of CHIP TPR specificity where the contribution of P5–P2 is denoted by the size of the circle (where Area ∝ ΔpK_i for a given Ala variant relative to CHIPOpt). CHIPScore is defined as the normalized sum of thermal shifts from the PSSCL DSF dataset for a given peptide sequence. **b,** Correlation (R^2) between CHIPScore and experimental pK_i (n=3, see Figure 1f) for the CHIPOpt alanine scanning library, as well as Hsp70 (red) and Hsp90 (blue) peptides. The degree of correlation was determined by linear regression. The fit and the 95% confidence interval are represented by the dotted and solid lines, respectively. **c,** The application of CHIPScore to the reference proteome identified proteins (black) with C-termini that are predicted to bind CHIP. Proteins that are predicted to be outside the cytosol or nucleus (dashed) would not be expected to interact with CHIP. Proteins previously identified as putative CHIP interaction partners are shown by arrows (Taipale et al.). **d,** Proteome wide prediction of latent CHIP binding C-termini likely to be unmasked by caspase activity, based on CHIPScore (x-axis) and caspase scoring (y-axis). Caspase scoring was based on a support vector machine (SVM) prediction function for caspase cleavage (Barkan et *al* https://modbase.compbio.ucsf.edu/peptide//). Hits (yellow) fall above a CHIPScore threshold of 1.79 (the value for Hsp90's MEEVD) and SVM threshold of (−0.464) (see methods and Supplementary Fig 5). **e,** The location of predicted CHIP interaction sites on caspase-6^{D179} and tau^{D421}. pIC_{50} values calculated from independent experiments (n=3) are plotted individually (open circles). Bars represent mean pIC_{50}. Error is plotted as SEM.

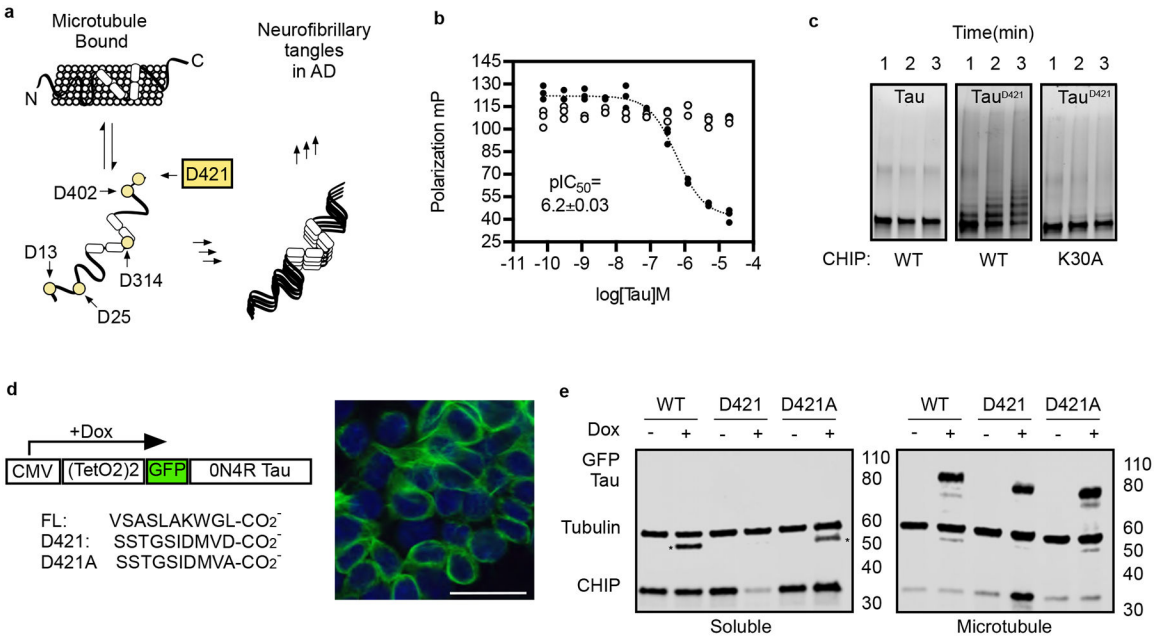

Fig. 4. Tau^{D421} specifically recruits CHIP

a, Schematic of how tau dissociates from microtubules and forms high-order aggregates during the progression of AD. Multiple caspase cleavages sites in tau, including D421, have been reported to accumulate in AD. **b,** In a competition binding FP experiment, tau^{D421} but not tau^{FL} displaces tracer bound to CHIP. Polarization (mP) is plotted for individual replicate samples (n=3) in a representative experiment. Reported pIC_{50} is mean of three independent experiments with error reported as SEM. **c,** *In vitro* ubiquitination experiment with CHIP(E3), UBCH5c(E2), Ubiquitin, and ATP demonstrates selective ubiquitination of tau^{D421} but not tau^{FL} by CHIP. Use of CHIP^{K30A} diminishes ubiquitination. Results are representative of three independent experiments. **d,** Tau^{FL}, tau^{D421}, or tau^{D421A} were stably expressed with an N-terminal GPF tag under the control of a Tet repressor ((TetO2)2) in TREx HEK293 cells. Representative live cell image shows GFP-tau (green, false color) associated with cytoskeletal structures. Scale bar is 30 μm. Nuclei are labeled with Hoechst (blue, false color). **e,** A microtubule fractionation assay for all three GFP-tau cell lines +/− 10 μg doxycycline for 72h after seeding. Probing with anti-GFP reveals that GFP-tau is in the microtubule-bound fraction (bottom panel). A low MW GFP positive band (*) was detected in the soluble fraction (top panel). Tubulin is distributed between the soluble and microtubule-bound fractions. CHIP is predominantly in the soluble fraction but is re-partitioned to the microtubule-bound fraction when tau^{D421} is expressed. Results are representative of three independent experiments. Uncropped blots in Supplementary Fig 9.

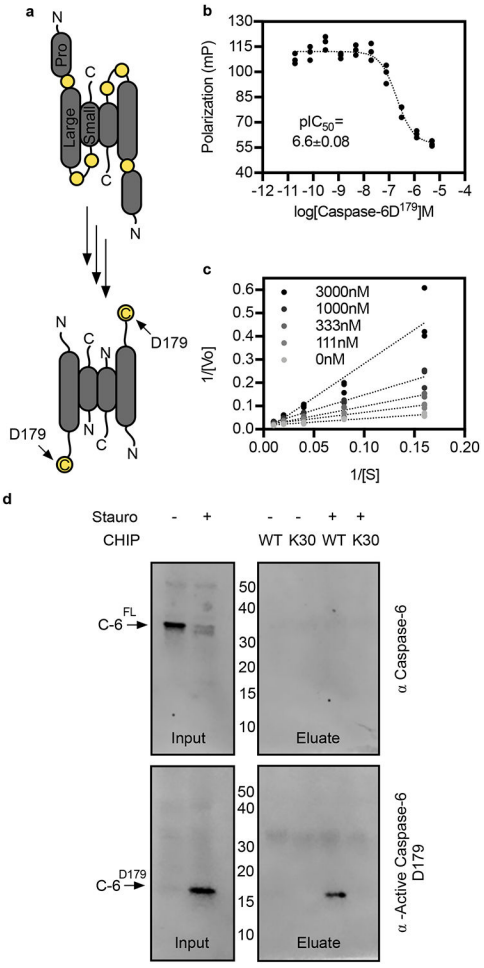

Fig. 5. CHIP specifically binds and inhibits mature caspase-6.

a, Caspase-6 is a constitutive homodimer that undergoes iterative proteolytic cleavages at three distinct sites (yellow circles) during maturation to yield a CHIP binding site (D179) at the C-terminus of the large subunit **b,** A competition binding FP experiment, caspase-6^{D179} displaces tracer bound to CHIP. Polarization (mP) is plotted for individual replicate samples (n=3) in a representative experiment. pIC_{50} is reported as a mean of three independent experiments with error reported as SEM. **c,** In a fluorogenic substrate cleavage assay, caspase-6^{D179} is competitively inhibited by increasing concentrations of CHIP. The reciprocal of initial velocity ($1/V_0$) is plotted relative to 1/[S] for individual replicate samples (n=3) in a given experiment. Results are representative of three independent experiments. **d,** Western blots show that caspase-6 zymogen (top panel, C-6^{FL}) does not pull down with recombinant biotinylated $CHIP^{WT}$ or $CHIP^{K30A}$ from Jurkat cell lysate. Caspase-6^{D179} is specifically generated in cells treated with staurosporin (1 μM) for 2h and is enriched in eluates from $CHIP^{WT}$ but not $CHIP^{K30A}$ (bottom panel, C-6^{D179}). Results are representative of three independent experiments. Uncropped blots in Supplementary Fig 9.

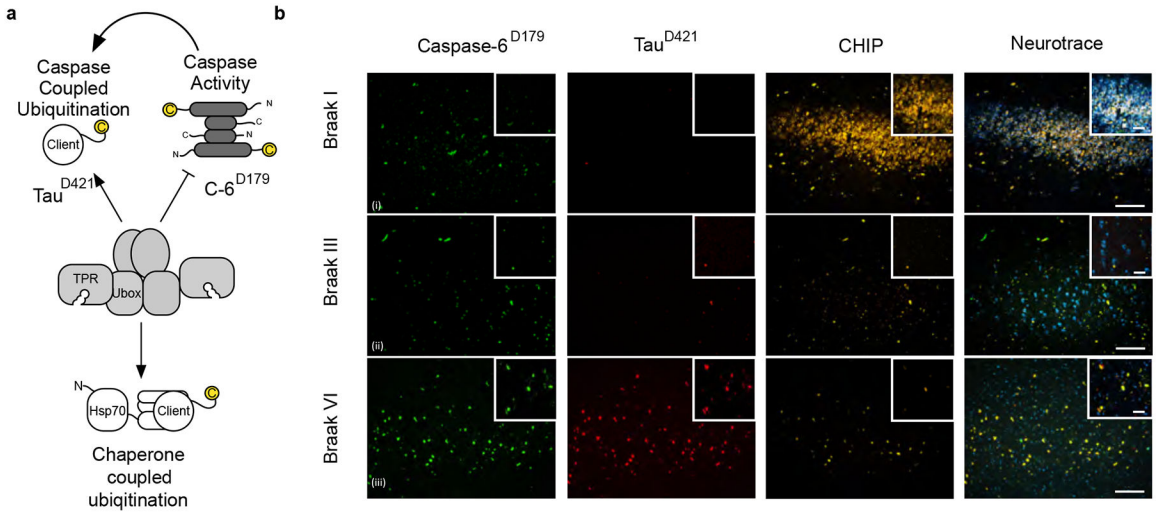

Fig. 6. CHIP interactions at latent C-termini suggest a role in the progression of AD

a, An integrated model of expanded CHIP functions including chaperone- and caspase-coupled ubiquitination of tau (MAPT^{D421}), as well as inhibition of caspase-6. **b,** Immunofluorescence signals and high-magnification insets of caspase-6^{D179} (green), tau^{D421} (red) and CHIP (yellow) positive neurons (blue Neurotrace/Nissl) in the hippocampal area CA1 of human brains from early (Braak I), middle (Braak III) and late (Braak VI) stages of AD. Scale bars: 50 μm; insets: 10 μm. Qualitative analysis for this study was conducted based on trends within the three samples presented in this figure.